

## Chromospheric Internetwork Oscillations at Various Locations of the Quiet Sun \*

Zong-Jun Ning<sup>1,2</sup> and Ming-De Ding<sup>1</sup>

<sup>1</sup> Department of Astronomy, Nanjing University, Nanjing 210093; [ningzongjun@hotmail.com](mailto:ningzongjun@hotmail.com)

<sup>2</sup> Purple Mountain Observatory, Chinese Academy of Sciences, Nanjing 210008

Received 2004 December 14; accepted 2005 March 5

**Abstract** We analyze oscillation behaviours in chromospheric internetwork regions using spectral observations of the C II 1334 Å line obtained with the Solar Ultraviolet Measurements of Emitted Radiation spectrograph (SUMER) aboard Solar and Heliospheric Observatory (SOHO). Three areas,  $26 \times 120$  arcsec<sup>2</sup> each, at the various latitudes from the disk center to the north polar coronal hole, were rastered with a cadence of about 40–60 s in the solar minimum year. We obtained the time evolution of two-dimensional (2D) line intensity, continuum and line core shift. The continuum and the line shift show  $\sim 3$  min chromospheric oscillations in the internetwork regions underlying the coronal hole as well as at the disk center. We find that the C II 1334 Å line shift oscillates with an average speed of  $\sim 1.7$  km s<sup>-1</sup>, independent of the latitude, while its coherent scale decreases with latitude. On the other hand, the oscillation amplitude of the continuum around the 1334 Å and the phase delay between the Doppler shift and continuum slightly increase with latitude.

**Key words:** Sun: chromosphere — Sun: oscillations

### 1 INTRODUCTION

The chromosphere of the quiet Sun displays a distinct network appearance identical to supergranules. Its cells are the internetwork regions where the field is weaker. These structures are consistent with two types of underlying photospheric magnetic flux: network field and internetwork field, the two types of magnetic topology on the quiet Sun (e.g. Wang 1988). Proper motions in the supergranular cell (internetwork) push the magnetic flux to concentrate along the boundary (network). Thus the magnetic flux is stronger there, which is thought to be the physical reason that the network structure shows an enhanced emission than the internetwork at the top of the solar atmosphere. These atmosphere networks have lifetimes of the order of  $\sim 10$  hours, the same as the underlying magnetic networks. At the chromospheric level, Lites

---

\* Supported by the National Natural Science Foundation of China.

et al. (1993) found two different types of oscillation in the network and internetwork:  $\sim 3$  min internetwork oscillations, and longer-period oscillations with a dominant period of  $\sim 5$ – $20$  min in the network regions. These results were further demonstrated by the space-based observations of extra-ultraviolet (EUV) spectral lines from SUMER (Carlsson et al. 1997; Judge et al. 1997; Wikstol et al. 2000; Hansteen et al. 2000; Banerjee et al. 2001) and bandpass from TRACE (Transition Region and Coronal Explorer) (e.g. Muglach 2003; McAteer et al. 2004).

Although the network oscillations are frequently observed with the Doppler velocity of the chromospheric lines (e.g. Kneer & von Vexkull 1993; Lites et al. 1993; Carlsson et al. 1997; Judge et al. 1997), Curdt & Heinzel (1998) found intensity oscillations in Lyman lines in the network with periods near 7 min. Later, McAteer et al. (2002) reported chromospheric oscillation in the Network Bright Points (NBPs) with periods of 4–15 min using high resolution observations in Ca II  $K_3$ . The traditional view on this kind of long-periodic chromospheric network oscillation is that it is caused by magneto-gravity waves trapped there by a diverging magnetic flux tube (Lou 1995) or by kink or sausage waves propagating upward along magnetic flux tubes in the chromosphere (Banerjee et al. 2001; Hasan et al. 2003). Spectral observations of the chromospheric internetwork show that both the continuum and line Doppler velocity are oscillating with a dominant period around 3 min (Carlsson et al. 1997; Judge et al. 1997). Wikstol et al. (2000) also found that the intensity of the chromospheric line C II 1036 Å has an oscillation of the same period and a much smaller amplitude than the continuum emission of the internetwork regions. They studied the chromospheric internetwork oscillations using the lines formed at different levels. They found that the oscillation in the 1036 Å neighboring continuum (formed in the middle chromosphere) preceded by  $\sim 50$  s that of the C II 1037 Å line (formed in the upper chromosphere/lower transition region), which in turn precede by 4 s the oscillation of the O VI 1031 line (formed in the upper transition region/lower corona). They concluded that the chromospheric internetwork oscillations are a signature of upward-propagating sound waves from the photosphere up to  $\sim 1$  Mm (Lites et al. 1993) and up to the 2 Mm level at the base of the corona.

Previous documented observations made by SUMER spectral or TRACE bandpass, focused on the solar disk center, were either in a quiet region or in an equatorial coronal hole (e. g., McIntosh et al. 2004). At present, our knowledge is still poor on the behaviour of chromospheric oscillation in internetwork around the poles, and especially, underlying the polar coronal hole. Marsh et al. (2003) studied the quasi-periodic variability across a solar coronal hole region using EUV lines covering the temperature range of  $\log T_e = 5.3$ – $6.1$  K, pertaining to the corona level. In this paper, we study the behaviour of chromospheric oscillation in internetwork regions at three different latitudes from the center to the poles. Our observations are made with a single slit not pointing at one position but scanning over a small zone with a high cadence.

## 2 OBSERVATIONS AND DATA REDUCTION

The data described here were made with SUMER (Wilhelm et al. 1995, 1997; Lemaire et al. 1997) on 24 and 27 June 1996 during the solar minimum year. The detailed observations are summarized in Table 1. These positions are the initial slit locations before the scan. For example, the sequence A<sub>1</sub> started at  $Y_0=0$ ,  $X_0=-2.25$  arcsec (position 1), the sequence A<sub>2</sub> at  $Y_0=500$ ,  $X_0=479.81$  arcsec (position 2), the sequence A<sub>3</sub> at  $Y_0=823$ ,  $X_0=97.81$  arcsec (position 3). Figure 1 shows the SUMER slit positions 1, 2 and 3 on the solar disk superimposed on the Michelson Doppler Image (MDI; Scherrer et al. 1995) image taken at 1996 June 24, 03:16 UT (Fig. 1a), and on the Extreme ultraviolet Imaging Telescope (EIT) 195 Å image taken at 1996 June 27, 19:32 UT (Fig. 1b). The polar coronal holes are clearly shown as the dark regions at the two poles. The northern polar coronal hole has a larger area than the southern one on June 27. For each position, an area of  $26 \times 120$  arcsec<sup>2</sup> was chosen to be observed with SUMER for

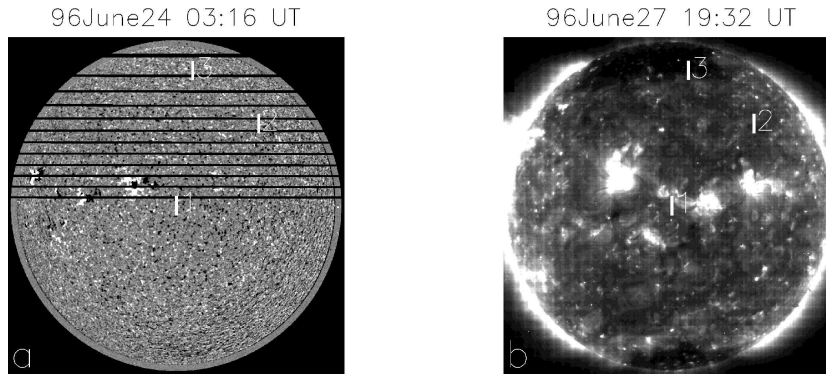


**Fig. 1** Three positions of SUMER slit superimposed on (a) MDI magnetic and (b) EIT 195 Å full-disk images. The first one (slit center  $X_0=0$ ,  $Y_0=0$ ) is near the solar disk center, the second ( $X_0=500$ ,  $Y_0=500$ ) is between the disk center and limb, and the third ( $X_0=100$ ,  $Y_0=823$ ) is at the north coronal hole (the polar dark regions on EIT 195 Å). North is up and west is to the right. Dark bars mark areas lacking MDI data.

**Table 1** Data set used in this paper obtained with SUMER during June 1996

No.	Date	Start (UT)	End (UT)	Slit position ( $X_0$ , $Y_0$ )	Step No.	Step size (arcsec)	Exp. time (s)
A <sub>1</sub>	24/06/96	03:21	04:02	(-2.25, 0)	6	1.13	5
B <sub>1</sub>	24/06/96	04:02	04:39	(-3.38, 0)	8	1.13	5
C <sub>1</sub>	24/06/96	04:40	05:15	(-2.25, 0)	6	1.13	10
A <sub>2</sub>	27/06/96	00:45	01:25	(479.81, 500)	6	1.13	5
B <sub>2</sub>	27/06/96	01:25	02:03	(496.69, 500)	8	1.13	5
C <sub>2</sub>	27/06/96	02:04	02:38	(497.81, 500)	6	1.13	10
A <sub>3</sub>	27/06/96	03:08	03:48	(97.81, 823)	6	1.13	5
B <sub>3</sub>	27/06/96	03:49	04:26	(96.69, 823)	8	1.13	5
C <sub>3</sub>	27/06/96	04:27	05:02	(97.81, 823)	6	1.13	10

three types of sequences with different exposure times and step numbers. Denote by A, B and C the three sequence and the subscripts 1, 2 and 3 the three positions mentioned above: A<sub>1</sub>, B<sub>1</sub>, C<sub>1</sub> represent the observations at the three continuous periods at the position 1; A<sub>2</sub>, B<sub>2</sub> and C<sub>2</sub> for position 2; A<sub>3</sub>, B<sub>3</sub> and C<sub>3</sub> for position 3.

Each area was rastered from east to west with a cadence of about 40–60 s for three continuous periods of over half an hour each. In half an hour, the Sun rotates about  $\sim 5$  arcsec near the disk center and  $\sim 1$  arcsec in the coronal hole, so the last scan is offset about  $\sim 5$  (position 1) or  $\sim 1$  (position 3) arcsec from the first scan in each period. Our data consists of stigmatic images acquired by SUMER along its  $1 \times 120$  arcsec<sup>2</sup> slit with a resolution of 1 arcsec in the S–N direction. Figure 2 gives the area near disk center superimposed on low resolution MDI images that are close in time to the beginning and end of the SUMER sequences on 24 June 1996. The three boxes from west to east correspond to the three regions rastered with three types of SUMER sequences, A<sub>1</sub>, B<sub>1</sub> and C<sub>1</sub>, in Table 1. The width of each box covers the entire area on the rotating solar disk swept by the slit during the whole period. For example, the dashed box for the sequence A<sub>1</sub> has a width of  $\sim 12.3$  arcsec, which is made up of 5.63 arcsec of area

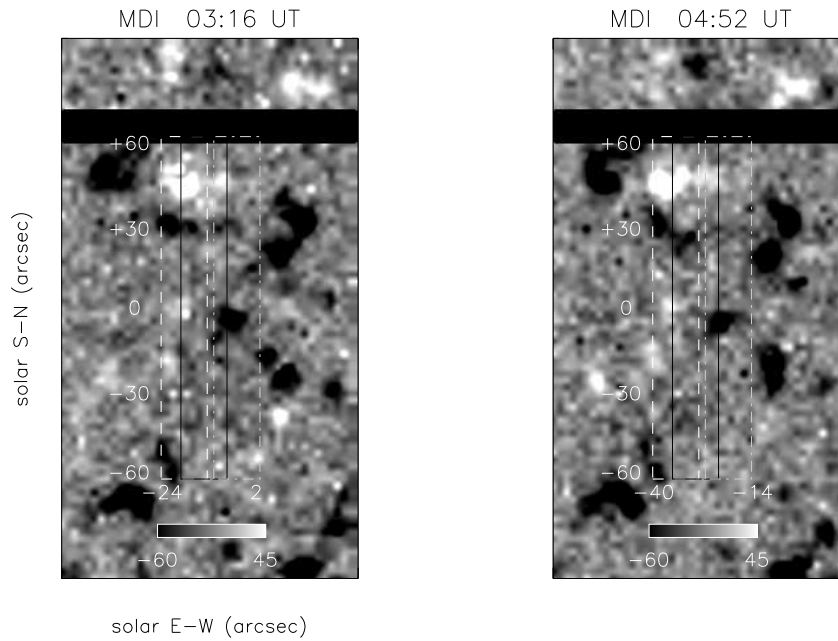


**Fig. 2** First area near the solar disk center (position 1) superimposed on low resolution MDI images, on 1996 June 24. The three boxes from west to east, correspond to SUMER scanning for the three periods  $A_1$ ,  $B_1$  and  $C_1$  in Table 1. The magnetic field strength is in Gauss.

covered by the scanning slit plus  $\sim 6.7$  arcsec, the area due to solar rotation between 03:21 and 04:02 UT. As can be seen, these regions cover several magnetic network lanes and internetwork regions. The magnetic field structure is stable during the SUMER raster periods, as shown by two panels in Fig. 2, separated by 96 min.

In each period, small raster scans, either 5.63 or 7.88 arcsec wide in the E–W direction, were made. The rasters were made with 6 or 8 steps of size 1.13 arcsec, and with an exposure time of either 5 s or 10 s depending on the observing sequence. In order to improve the time resolution, the data were first recorded at the odd-number locations and then at the even-number locations. For example, the sequence  $A_1$  started at  $Y_0=0$ ,  $X_0=-2.25$  arcsec (position 1), then successively moving to west,  $X_0=0$ , 2.25,  $-1.13$ , 1.13 and 3.38 while  $Y_0$  remains fixed, with a step size of 2.25 arcsec, the total of six steps taking 40 s (from 03:21:00 to 03:21:40 UT) for the first cadence, and for a total of 40 cadences between 03:21 and 04:02 UT on June 24. We found that the temporal change is much smaller than the change along the scanning direction (E–W) after many small rasters. Therefore, in the following analysis, we have filled the missing raster locations in each scan with the average of the spectra taken at the same location just before and after the scan. For example, the missing locations  $X_0=-1.13$ , 1.13, 3.38,  $-2.25$ , 0 and 2.25 arcsec in the first cadence  $A_1$  were so filled. Thus we obtain two new cadences with six steps between  $-2.25$  and 3.38, at one half initial step size (1.13 arcsec), from one primary cadence. Thus, the time resolution is improved to 20 s for the new cadence from the observational 40 s per original cadence of the sequence  $A_1$ . A detailed description of the data from these series of SUMER observations has been presented in Innes et al. (1997) and Ning et al. (2004).

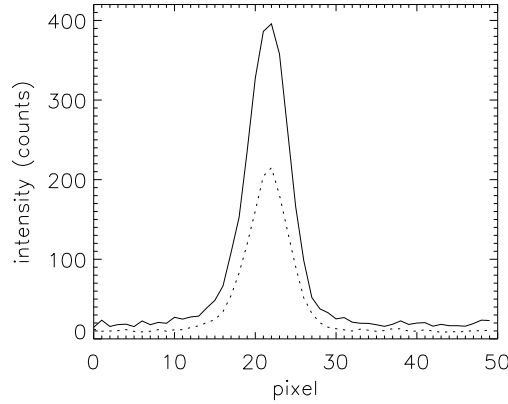


**Fig. 3** Average emission around the C II 1334 Å line from internetwork regions around (−40) at the sequence A<sub>1</sub> (see Fig. 4) in the quiet Sun (solid line) and around 823 at A<sub>3</sub> (see Fig. 4) in the coronal hole region (dotted line). The line center is located at 22 pixel.

The line C II 1334 Å formed in the upper chromosphere/lower transition region, is used for all of SUMER observation sequences here in order to compare the oscillation behaviours from various locations along the latitude. C II 1334 Å is a strong isolated line without any blends surrounding (Curdt et al. 2001) and has been used in study of chromospheric oscillations before (e.g. Hansteen et al. 2000). Actually, our observational window includes only this line. Figure 3 shows the spectral profiles of the C II 1334 Å line from the internetwork regions in the quiet Sun and coronal hole.

Two wavelength-integrated quantities, the total intensity  $I_{\text{tot}}$  and the line shift velocity  $\bar{v}$  are computed with the following Eqs. (1) and (2) (Carlsson et al. 1997):

$$I_{\text{tot}} = \int_{\lambda_0 - \Delta\lambda}^{\lambda_0 + \Delta\lambda} (I_\lambda - I_{\text{cont}}) d\lambda, \quad (1)$$

$$\bar{v} = \int_{\lambda_0 - \Delta\lambda}^{\lambda_0 + \Delta\lambda} (I_\lambda - I_{\text{cont}}) v_\lambda d\lambda / I_{\text{tot}}, \quad (2)$$

where  $I_{\text{cont}}$  is the background continuum intensity, which is computed by interpolating the average counts in two windows on either side of the line, between pixels 0–5 and 45–49. All intensity data are given in counts per exposure on the detector. The Doppler velocity  $\bar{v}$  is given in units of  $\text{km s}^{-1}$ , and  $v_\lambda = c(\lambda - \lambda_0)/\lambda_0$ , where  $c$  is light speed in vacuum, and  $\lambda_0$  is the rest wavelength of line center, i.e., the center of the line profile averaged over the quiet regions. We analyzed all the profiles to obtain the 2D time evolution of the total intensity and line shift velocity of C II 1334 Å core, and the continuum emission near this wavelength.

### 3 RESULTS

#### 3.1 Identification of the Internetwork Regions

As mentioned before, the chromospheric internetwork and network structures are counterparts of underlying magnetic structures on the photosphere. The chromospheric lines show an en-

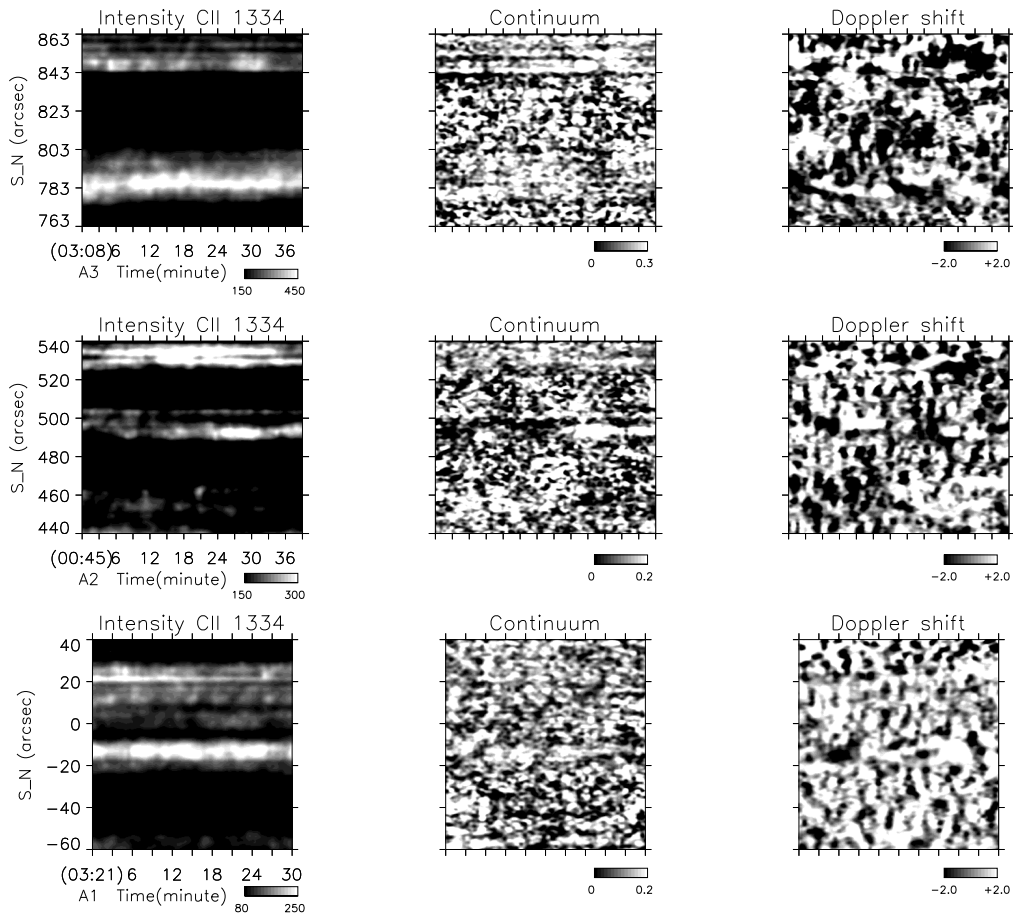


**Fig. 4** Time variations of total intensity, continuum and line core shift (blank is blue-shift and white is redshift) of CII 1334 Å from the slit at a certain position in E–W direction for the three sequences A<sub>1</sub>, A<sub>2</sub> and A<sub>3</sub> in Table 1.

hanced emission over the magnetic network regions usually known as NBPs (e.g., Falchi et al. 1987). The dark regions among the NBPs are thought to be the internetwork. Actually, the network and internetwork structures exist not only at the chromosphere level, but all way from the lower chromosphere through the transition region to the lower corona. Gallagher et al. (1998) examined the network emissions on the different lines formed from the various levels and found that the emission is more concentrated in the transition region than in the chromosphere or corona. So far, an exact distinction between network and internetwork emission is still lacking. A rough lining-up by eye is the usual means to distinguish the internetwork from the bright network (e.g., Wikstol et al. 2000). Meanwhile, these emission structures can be identified by the underlying magnetic internetwork and network regions.

We make a slanted section from each 2D time evolution data to obtain the oscillating behaviours for a given position of the slit in the E–W direction. Figure 4 shows sample time variations of total intensity, continuum and line shift from the first slit scan position along the

E–W direction with sequences  $A_1$ ,  $A_2$  and  $A_3$ . For example,  $A_1$  shows the oscillating behaviours from the slit position at the west edge of the white dashed box in Fig. 2. These sections are chosen to be related with the solar rotation speed there. The dashed lines in Fig. 5 represent the solar rotation speeds of 1 arcsec per 6 min (position 1), 1 arcsec per 12 min (position 2) and 1 arcsec per 32 min (position 3), respectively. These speeds are deduced under the assumption that the chromosphere maintains a quasi-rigid rotation with the solar disk. The top 20 arcsec data in Fig. 4 are lacking because of a noise there.

The internetwork regions are identified by the time variations of the  $\text{CII} 1334 \text{ \AA}$  total intensity (the first column in Figure 4) and by the underlying magnetic structures. Obviously, two magnetic network lanes are covered in the photospheric magnetic image in Fig. 2, where the  $\text{CII} 1334 \text{ \AA}$  line shows an enhanced emission above the surrounding internetwork regions in  $A_1$  (Fig. 4). The networks are bright during the observing periods because the underlying magnetic networks are stable. Thus we can acquire the internetwork regions directly according to the  $\text{CII}$  intensity brightness. For example, the regions between  $(-60)$ – $(-20)$ ,  $(-5)$ – $20$ , and  $30$ – $43$  for the sequence  $A_1$ , between  $400$ – $484$  and  $510$ – $528$  at  $A_2$ , between  $763$ – $773$  and  $798$ – $843$  at  $A_3$  along the slit direction are thought to be internetwork regions here.

### 3.2 Oscillation Coherent Scale

Figure 5 shows time variations of the continuum and the line shift along the E–W direction at the typical internetwork regions near  $-40$  arcsec at slit position 1, near  $470$  arcsec at slit position 2 and near  $825$  arcsec at slit position 3. These internetwork regions display distinct  $\sim 3$  min oscillating behaviours in the continuum as well as the Doppler velocity. At the disk

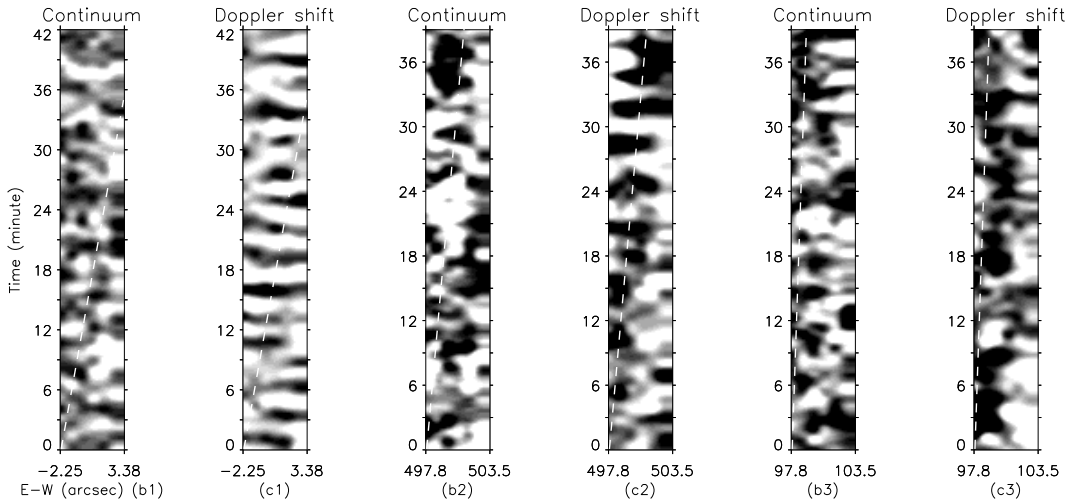


**Fig. 5** Time evolutions of the continuum and  $\text{CII} 1334 \text{ \AA}$  line shift (blank is blue-shift and white is redshift) along the E–W direction at the internetwork regions near  $(-40)$  along S–N at slit position 1 (see Fig. 2) for the  $A_1$  sequence ( $b_1$  and  $c_1$ ); at internetwork near  $470$  at slit position 2 for  $A_2$  ( $b_2$  and  $c_2$ ); at internetwork near  $825$  at slit position 3 for  $A_3$  ( $b_3$  and  $c_3$ ). The dashed lines represent the solar rotation speeds at the corresponding positions.

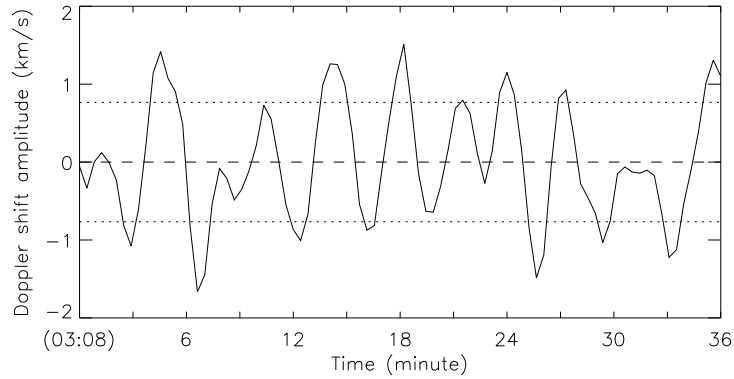


**Fig. 6** Average oscillation profile in the internetwork near  $-40$  arcsec for the sequence  $A_1$  in Fig. 4. The average value is plotted in dashed line, and the dotted lines are the average value plus and minus a standard deviation, which is thought to be the oscillation amplitude of the Doppler velocity (redshift positive).

center, the Doppler velocities are oscillating with a typical coherent scale over a few arcsec, up to the entire viewing window (about 6 arcsec) along the E–W direction. The coherent scales of the Doppler oscillations are distinctly different at the disk center and at high latitude: the scale decreases with increasing latitude, from  $\sim 6$  arcsec near the center to  $\sim 3$  arcsec below the coronal hole. This tendency also exists in Fig. 4 for the time variation along the S–N direction. The continuum oscillations show a coherent scale about 2–4 arcsec, sometimes up to 6 arcsec, which is of the same order as the 3–8 arcsec in the chromospheric internetwork regions documented by Carlsson et al. (1997). Meanwhile, the coherent scale of continuum oscillations is independent of the latitude. The same large coherent scale is found in the Doppler shift oscillations near the disk center with the same phase along the E–W direction during the observing period for the sequence  $A_1$ . However, the Doppler shift is oscillating with a different or the opposite phase along the E–W direction in the internetwork underlying the coronal hole.

### 3.3 Oscillation Amplitude and Phase Difference between the Continuum and Doppler Shift

For the internetwork regions, we calculated the oscillation amplitudes of the continuum and Doppler velocity and we obtain the distribution of these parameters along the latitude. Figure 6 shows the time profile of Doppler shift oscillation (amplitude and standard deviation) in the internetwork near  $-40$  arcsec at slit position 1. Then we move to other locations along the latitude in the internetwork regions. Figure 7 gives these oscillating parameters as a function of the slit position measured away from the solar equator to the northern coronal hole, for the three SUMER sequences  $A_1$ ,  $A_2$  and  $A_3$  in Table 1. As mentioned before, they belong to the same sequences of SUMER raster, but at different observing periods, at positions 1, 2 and 3, respectively. We assume the oscillation behaviours are independent of the observing time. We also plot the phase difference between the continuum and line shift oscillations at each location. Usually, the continuum precedes the upward velocity (e.g. Wikstol et al. 2000). This parameter is calculated by cross-correlation. According to the time profile of continuum and

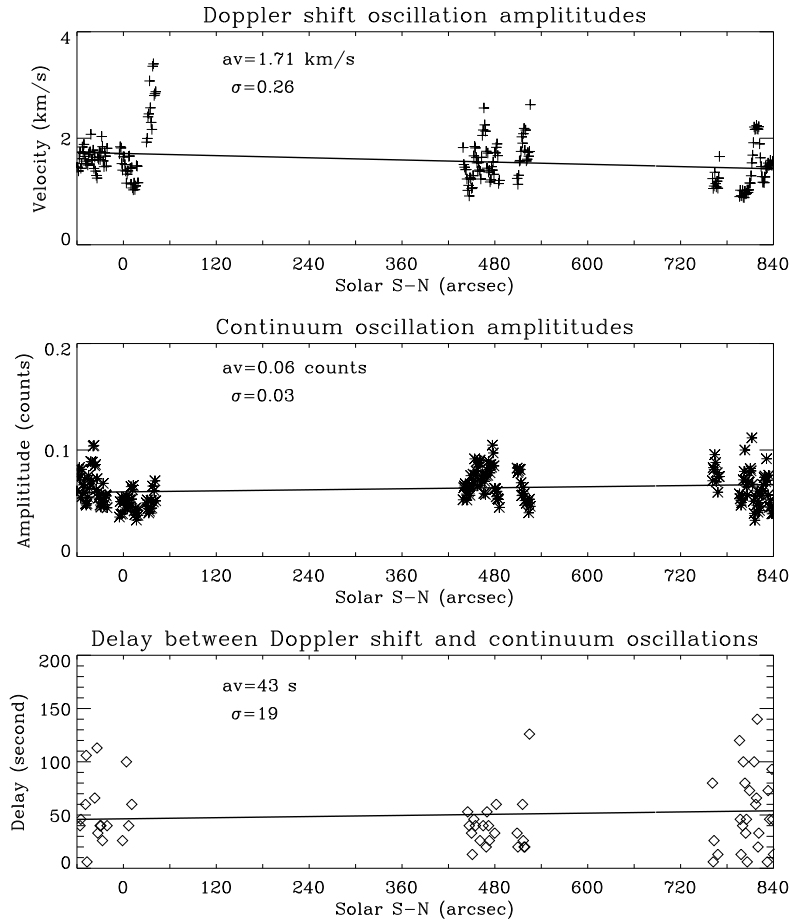


**Fig. 7** Oscillation amplitudes of the continuum and line core shift in internetwork regions, and phase difference between them as functions of the latitude from the equator to the north polar coronal hole. From left to right, the three groups of observational points correspond to the three SUMER slit positions  $A_1$ ,  $A_2$  and  $A_3$  in Table 1. The solid lines are linear fits to the observational points. Here ‘av’ and  $\sigma$  are average value and standard deviation for all data along the latitude, respectively.

Doppler velocity oscillations at each location, we move forward the Doppler velocity profile along the time axis to look for the maximum cross-correlation coefficient between them. The phase difference is computed by the number of pixels moved. They are thought to be in phase when the maximum coefficient appears without any shift of the two parameters. When one pixel of velocity is moved, the phase difference equals the time resolution of each raster scan, for example, 20 s at the sequence  $A_1$ . When two pixels are moved, the phase difference is then twice the time resolution, and so on.

Figures 8 and 9 show these parameters as a function along the latitude for the other two sets of sequences  $B_1, B_2, B_3$  and  $C_1, C_2, C_3$  in Table 1. They present the same results as Fig. 7 in the internetwork regions. First, the line shift of  $\text{CII } 1334 \text{ \AA}$  core is oscillating with an almost

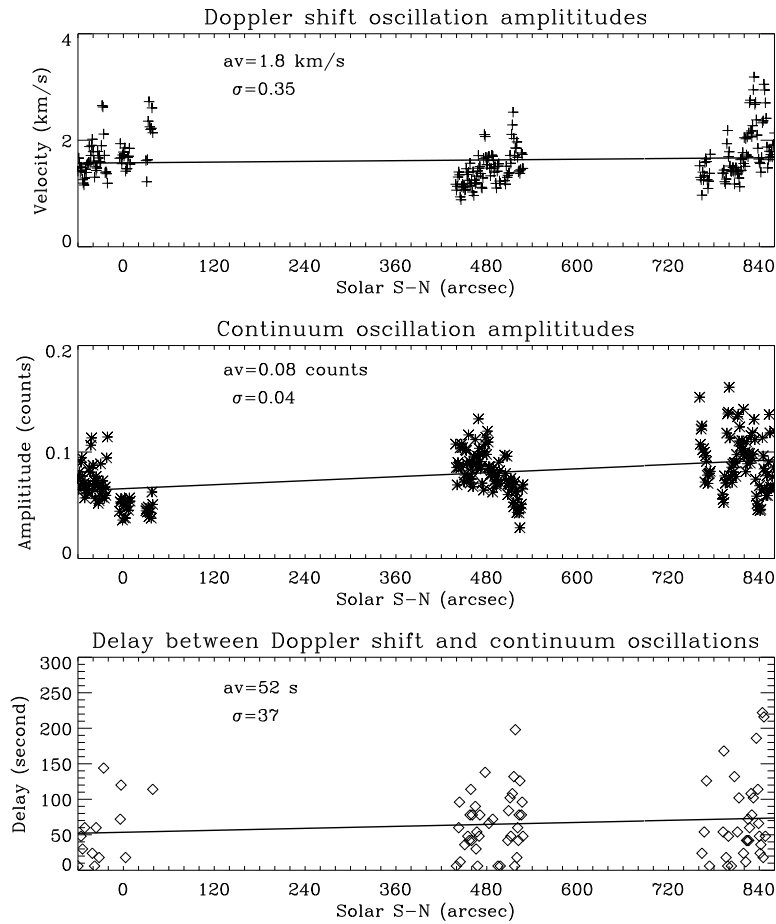


**Fig. 8** Same as Fig. 7 but for the three SUMER sequences B<sub>1</sub>, B<sub>2</sub> and B<sub>3</sub> in Table 1.

same amplitude from disk center to coronal hole, the average value of  $\sim 1.7 \pm 0.5 \text{ km s}^{-1}$ , which is the same order as in Lites et al. (1993), but less than the value of  $\sim 2.5 \text{ km s}^{-1}$  (the line CII 1334 Å as well) in Hansteen et al. (2000) and of  $3\text{--}5 \text{ km s}^{-1}$  (the line CII 1036 Å in Wikstol et al. 2000). Secondly, the continuum is oscillating with a larger amplitude (on average,  $\sim 0.09$  counts per arcsec<sup>2</sup>) in the coronal hole than near the disk center (average value  $\sim 0.06$  counts per arcsec<sup>2</sup>). Over the three positions along the latitude the average value is  $\sim 0.07$  counts per arcsec<sup>2</sup>. Finally, the phase difference between them increases slightly from the equator ( $\sim 50$  s) to the north polar coronal hole ( $\sim 70$  s). The average value for all the data is  $\sim 53$  s, and this is the same order as the phase delay (40–60 s) found by Wikstol et al. (2000).

#### 4 DISCUSSION

It is widely thought that coronal holes have different features from the solar quiet region. They are associated with rapidly expanding magnetic fields, and are an apparent source of the fast solar wind (e.g. Krieger et al. 1973). Coronal holes are dominant near both poles in solar

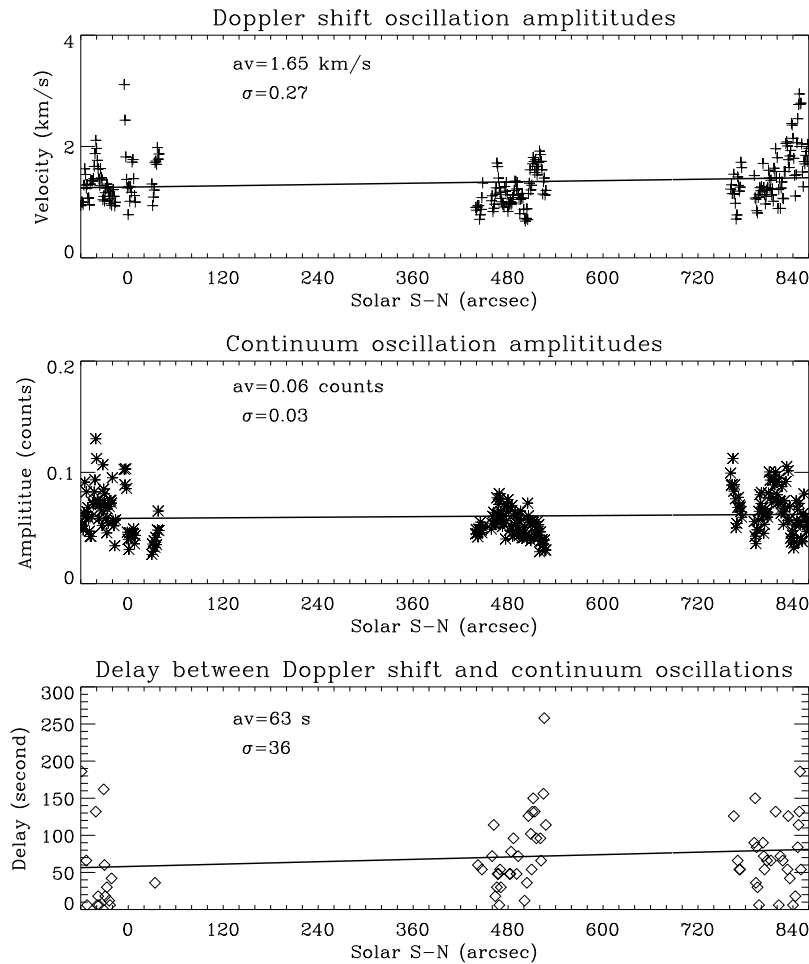


**Fig. 9** Same as Fig. 7 but for the three SUMER sequences  $C_1$ ,  $C_2$  and  $C_3$  in Table 1.

minimum years. They are invisible in chromospheric lines like the line CII analyzed here, but visible in coronal lines because of their smaller emission than the surrounding corona. Therefore, the oscillations investigated in this paper did not really refer to the coronal hole, rather, they refer to their underlying regions. We studied the chromospheric oscillations in the internetwork regions at various latitudes. We found that the coherent scale of the chromospheric Doppler oscillations decreases with increasing latitude, from more than 6 arcsec near the disk center to  $\sim 3$  arcsec below the polar coronal hole. This could be related with the plasma condition in the internetwork regions. McIntosh et al. (2004) studied the chromospheric oscillation inside and around an equatorial coronal hole observed by TRACE. They found that the plasma conditions inside are different from those on the hole boundary and also from the quiet Sun internetwork regions. The coronal hole interior plasma (with high plasma- $\beta$ ): at the base of the chromosphere, is largely hydrodynamic, which could result in the oscillating coherent scale being smaller in the internetwork underlying the coronal hole than in the quiet region near the disk center.

The issue of the coronal heating is one the mostly studied and still debated areas of solar physics. The conventional heating model is based on dissipation of magnetic energy at a current sheet (e.g. Schrijver & Title 2003; Solanki et al. 2003), or of Alfvén waves (e.g. Klimchuk et al. 2004; Moriyasu et al. 2004) propagating upward from the photosphere through the chromosphere/transition region to the coronal level. Some authors found that Alfvén waves excited by footpoint motions of a flux tube generate longitudinal modes (e.g., sound waves) by mode coupling (e.g. Hasan et al. 2003). The  $\sim 3$ -min chromospheric oscillation behaviours are thought to be observational evidence for the sound waves. Our results in this paper imply that the amplitude of this kind of wave is independent of the latitude and the average value of  $\sim 1.7 \pm 0.5 \text{ km s}^{-1}$  is the same at the disk center as in the high latitude. The oscillating amplitudes of the continuum and the phase delay increase slightly with the latitude, about the average values of  $\sim 0.07$  counts per arcsec<sup>2</sup> and  $\sim 53$  s.

**Acknowledgements** The SUMER project is financially supported by DLR, CNES, NASA and the ESA PRODEX programme (Swiss contribution). SUMER is part of SOHO, the Solar and Heliospheric Observatory, of ESA and NASA. This work was also supported by NKBRSF under grant G20000784, by NSFC under grant 10025315, 10221001, 10333030 and 10333040, a grant from TRAPOYT, and a postdoctoral grant 0201003005 and Jiangsu Province postdoctoral project.

## References

- Carlsson M., Judge P. G., Wilhelm K., 1997, *ApJ*, 486, L63  
 Banerjee D., O’Shea E., Doyle J. G., et al., 2001, *A&A*, 371, 1137  
 Curdt W., Brekke P., Feldman U. et al., 2001, *A&A*, 375, 591  
 Curdt W., Heinzel P., 1998, *ApJ*, 503, L95  
 Falchi A., Falciani R., Tozzi G. P. et al., 1987, *Sol. Phys.*, 114, 29  
 Gallagher P. T., Phillips K. J. H., Harra-Murnion L. K. et al., 1998, *A&A*, 335, 733  
 Hansteen V. H., Betta R., Carlsson M., 2000, *A&A*, 360, 742  
 Hasan S. S., Kalkofen W., van Ballegoijen A. A. et al., 2003, *ApJ*, 585, 1138  
 Innes D. E., Inhester B., Axford W. I. et al., 1997, *Nature*, 386, 811  
 Judge P., Carlsson M., Wilhelm K., 1997, *ApJ*, 490, L195  
 Klimchuk J. A., Porter L. J., Sturrock P. A., 2004, *Sol. Phys.*, 221, 47  
 Kneer F., von Uexkull M., 1993, *A&A*, 274, 584  
 Krieger A. S., Timothy A. F., Roelof, E. C., 1973, *Sol. Phys.*, 29, 505  
 Lou Y., 1995, *MNRAS*, 274, L1  
 Lemaire P., Wilhelm K., Curdt W. et al., 1997, *Sol. Phys.*, 170, 105  
 Lites B. W., Rutten R. J., Kalkofen W., 1993, *ApJ*, 414, 345  
 Ning Z. J., Innes D., Solanki S., 2004, *A&A*, 419, 1141  
 Marsh M. S., Walsh R. W., Bromage B. J. I., 2002, *A&A*, 393, 649  
 McAteer R. T. J., Gallagher P. T., Bloomfield D. S. et al., 2004, *ApJ*, 602, 436  
 McAteer R. T. J., Gallagher P. T., Williams D. R. et al., 2002, *ApJ*, 567, L165  
 McIntosh S. W., Fleck B., Tarbell T. D., 2004, *ApJ*, 609, L95  
 Moriyasu S., Kudoh T., Yokoyama T. et al., 2004, *ApJ*, 601, L107  
 Muglach K., 2003, *A&A*, 401, 685  
 Scherrer P. H., Bogart R. S., Bush R. I. et al., 1995, *Sol. Phys.*, 162, 129  
 Schrijver C. J., Title A. M., 2003, *ApJ*, 597, L165  
 Solanki S. K., Lagg A., Woch J. et al., 2003, *Nature*, 425, 692  
 Wilhelm K., Curdt W., Marsch E. et al., 1997, *Sol. Phys.*, 170, 75  
 Wilhelm K., Lemaire P., Curdt W. et al., 1995, *Sol. Phys.*, 162, 189  
 Wikstøl Ø., Hansteen V. H., Carlsson M., Judge P. G., 2000, *ApJ*, 531, 1150  
 Wang H., 1988, *Sol. Phys.*, 116, 1